Smart Structures and Systems, Vol. 4, No. 2 (2008) 247-259
DOI: http://dx.doi.org/10.12989/sss.2008.4.2.221

Use of copper shape memory alloys in retrofitting historical monuments

S. El-Borgi*, M. Neifar, M. Ben Jabeur, D. Cherif and H. Smaoui

Applied Mechanics and Systems Research Laboratory, Tunisia Polytechnic School, B.P. 743, La Marsa 2078, Tunisia

(Received July 6, 2007, Accepted October 8, 2007)

Abstract. The potential use of Cu-based shape memory alloys (SMA) in retrofitting historical monuments is investigated in this paper. This study is part of the ongoing work conducted in Tunisia within the framework of the FP6 European Union project (WIND-CHIME) on the use of appropriate modern seismic protective systems in the conservation of Mediterranean historical buildings in earthquake-prone areas. The present investigation consists of a finite element simulation, as a preliminary to an experimental study where a cantilever masonry wall, representing a part of a historical monument, is subjected to monotonic and quasi-static cyclic loadings around a horizontal axis at the base level. The wall was retrofitted with an array of copper SMA wires with different cross-sectional areas. A new model is proposed for heat-treated copper SMAs and is validated based on published experimental results. A series of nonlinear finite element analyses are then performed on the wall for the purpose of assessing the SMA device retrofitting capabilities. Simulation results show an improvement of the wall response for the case of monotonic and quasi-static cyclic loadings.

Keywords: copper shape memory alloy; nonlinear finite element analysis; crack modeling; monotonic static loading; cyclic quasi-static loading.

1. Introduction

The WIND-CHIME Project, sponsored by the European Union, aims at the preservation and conservation of Mediterranean historical buildings in earthquake-prone areas by means of appropriate modern seismic protective systems. The building under investigation in Tunisia is the Zaouia of Sidi Kassem Djilizi, located near downtown Tunis.

The retrofitting technique proposed here attempts to take advantage of the special behavioral features of shape memory allows (SMA). Indeed, these outstanding properties gave birth to several industrial applications such as biomechanical implants, actuators, and vibration isolators (Lagoudas 1999), and research efforts continue to be deployed to extend the range of applications of SMAs. The behavior of SMAs is the result of a solid-solid phase transformation known as martensitic transformation. At the macroscopic scale this phase transformation gives rise to many types of behaviors that do not exist in traditional materials (Patoor 1990, 1994). Among these properties, the following are particularly useful for retrofitting of masonry structures, that is

- The ability to develop recoverable strain orders of magnitude higher than typically seen in

*Corresponding Author, E-mail: sami.elborgi@gnet.tn

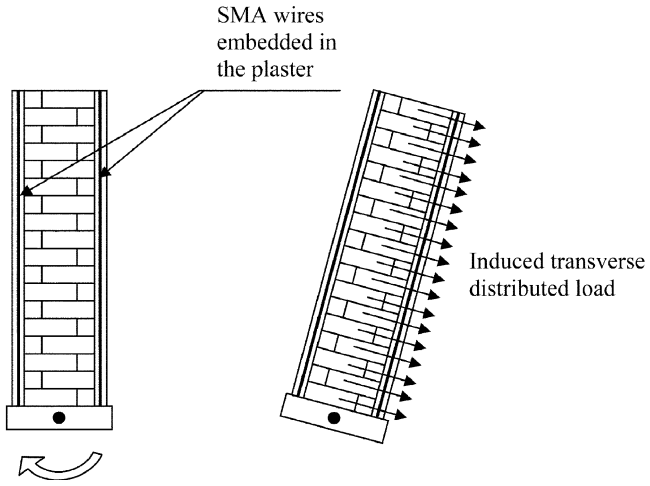

Fig. 1 Schematic of the planned experimental test

traditional materials (superelastic effect), which allows for strains large enough to be compatible with the large motion of interacting rigid bodies that can occur in damaged masonry structures.

• The presence of hysteresis which is an indicator of energy dissipation capability that provides a potential for using SMAs as damping devices.

The present investigation is preliminary to an experimental study where a model of a cantilever wall will be subjected to monotonic and quasi-static cyclic loadings around a horizontal axis at the base level as depicted in Fig. 1. With this simple mechanism, one is capable of achieving combined in plane and transverse distributed loadings, with the latter component being periodic, which conveniently approaches earthquake type excitation without dynamic shaking equipment. Simulation of the experiment aims at designing the SMA device and assessing its retrofitting capabilities.

2. Description of structure and material characterization

The monument under investigation (El-Borgi 2006) comprises numerous masonry walls that are suffering various types of damage, often in the form of long cracks (Fig. 2). The walls are made of stone blocks and mortar joints and are coated with plaster on both sides. The blocks material is predominantly sandstone. The selected wall has a height of 7.70 m, a length of 7.75 m and a thickness of 0.50 m. A series of experimental tests were conducted to determine the mechanical properties of stone and mortar samples extracted from the monument. Based on compression tests and indirect tensile tests on stone specimen, bloc compressive and tensile strengths are evaluated at $f_{bc} = 18$ MPa and $f_{bt} = 4.9$ MPa respectively. For mortar, compressive and tensile strengths are estimated at $f_{mc} = 2.7$ MPa and $f_{mt} = 0.42$ MPa respectively. Equivalent properties for masonry are determined based on available empirical rules (Syrmakezis 1995). A key parameter is the compressive strength fwc which is estimated at 4.5 MPa based on values given by several alternative formulae, ranging between 2 and 6 MPa. The modulus of elasticity is given by $E_w = 1000\, f_{wc} = 4500$ MPa. Poisson's ratio is taken as 0.16. Finally, the tensile strength is estimated at $f_{wt} = 2\, f_{mt}\, /3 = 0.28$ MPa.

Fig. 2 Cracks in one of the walls of Zaouia of Sidi Kassem Djilizi

3. Description of retrofitting device

The proposed reinforcement mechanism consists of attaching a series of vertical SMA wires to the sides of the wall, spanning its height from floor to ceiling. The wires can be attached with some clearance away from the wall by means of supports that are rigidly fixed to the wall (Fig. 2). They can also be completely bonded to the wall by being either glued to the surface or embedded in the plaster coating. In the present investigation the latter scenario is assumed, and this implies that the longitudinal strain will be identical in the wire and the surrounding wall material.

4. Finite element model

A three-dimensional finite element model of the masonry wall is constructed using eight-node solid elements, with linear interpolation. This wall is assumed to be clamped at its base. The Shape Memory Alloys wires are modelled using 1D frame elements embedded in the solid elements which are referred to as mother elements. The embedded elements do not have degrees of freedom of their own and their formulation is based on the assumption of perfect bond between masonry and SMA. This means that the axial strain in the SMA reinforcement can be computed from the displacement field of mother elements. The entire model, shown in Fig. 3, comprises a total of 216 solid elements and 343 nodes.

In this study, the multi-directional fixed smeared crack model (De Borst 1987) was adopted to model cracking in masonry. The model consists of a linear tension softening diagram, shown in Fig. 4, with constant tension cut-off, as depicted in Fig. 5, in addition to shear retention. The softening diagram is

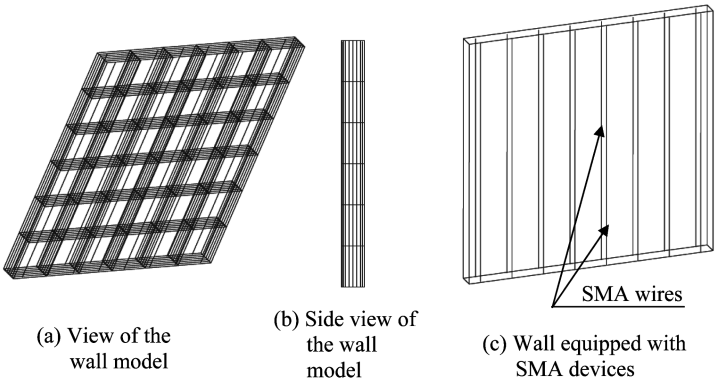

Fig. 3 Finite element model of the wall with SMA devices

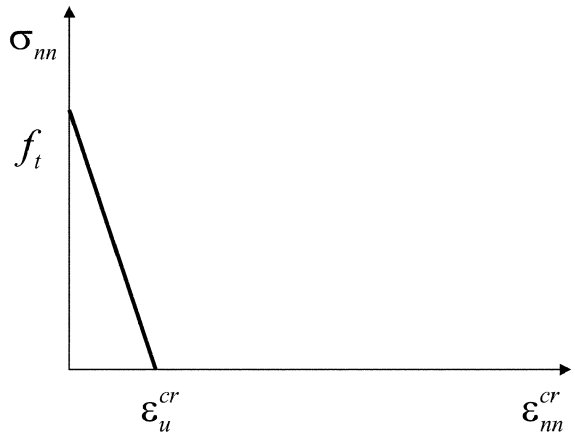

Fig. 4 Masonry tension softening diagram

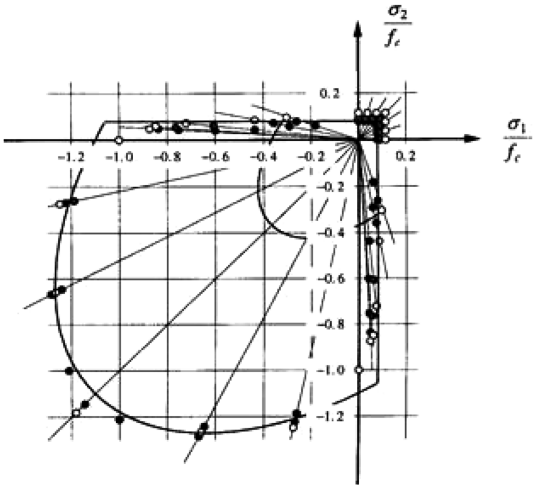

Fig. 5 Masonry failure diagram

Table 1 Masonry properties used in finite element model

Young modulus E	4500 MPa
Poisson's ratio ν	0.16
Mass density ρ	2700 kg/m^3
Yield stress	4.5 MPa
Tensile strength	0.28 MPa
Constant shear retention factor	0.2
Ultimate strain of diagram	0.008

defined by the masonry uniaxial tensile strength f_t and its ultimate tensile crack strain ε_v^{cr}. This diagram governs the behaviour of the material in the direction perpendicular to the crack once the maximum tensile stress is reached. The multi-directional fixed crack model is combined with a von Mises plasticity criterion (Boresi 2003) to model masonry in compression and crushing, as illustrated in Fig. 5. Table 1 gives the linear and nonlinear properties of the masonry used in the finite element model.

5. Modeling of copper shape memory alloys

According to (Casciati 2007), the temperature window of Ni-Ti shape memory alloys is too limited to cover realistic engineering applications (ie, the range of -20 °C to 80 °C). Therefore, it was proposed by the same reference that a more suitable option would be to use Cu-based shape memory alloys whose temperature window is consistent with most civil engineering applications. It was then decided to use this type of SMA has been retained for the present study.

5.1. SMA one-dimensional constitutive law

In all the constitutive laws cited in the literature (Brinson 1996), stress and temperature are chosen as control variables. Since the strain is generally determined first in a finite element method, a suitable algorithm had to be proposed for each behavior model, in order to compute the stress increment. The constitutive law adopted here for the SMA wire derives from Auricchio's 1D superelastic phenomenological law (Auricchio 1997), which is modified so that strain is used as control variable whereas the temperature is considered to be constant. In this way, the complexity of transformation correction required by stress controlled models is avoided. The resulting constitutive law is composed of two coupled laws: a mechanical and a kinetic laws.

5.1.1. Mechanical law

The total strain rate $\dot{\varepsilon}$ is decomposed into an elastic part $\dot{\varepsilon}^{el}$ and a transformation part $\dot{\varepsilon}^{tr}$

$$\dot{\varepsilon} = \dot{\varepsilon}^{el} + \dot{\varepsilon}^{tr} \tag{1}$$

To capture the phase transformation effects, the transformation strain ε^{tr} given by

$$\dot{\varepsilon}^{tr} = \dot{\xi}\dot{\varepsilon}^{tr}_{\max} \tag{2}$$

is introduced, where

$\dot{\xi}$ is the volume fraction change of detwinned martensitic phase,

$\varepsilon^{tr}_{\max}$ is the maximum uniaxial transformation strain,

The stress evolution is given by

$$\dot{\sigma} = E\dot{\varepsilon}^{el} \tag{3}$$

E is the equivalent Young modulus:

$$E = \xi E_M + (1-\xi)E_A \tag{4}$$

where

E_A is the austenite Young modulus

E_M is the martensite Young modulus

By substituting the elastic strain from Eq. (1). into Eq. (3), the following mechanical law is obtained:

$$\dot{\sigma} = E:(\dot{\varepsilon} - \dot{\varepsilon}^{tr}) \tag{5}$$

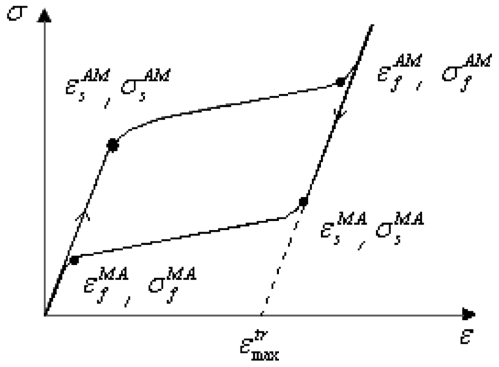

Fig. 6 SMA superelastic effect

5.1.2. Kinetic law

The kinetic law is employed to describe the evolution of the phase state for a given strain increment. One seeks to determine the rate of change $\dot{\xi}$ in the volume fraction of detwinned martensite as well as the rate of transformation strain. The parameters appearing in Fig. 6 showing the stress-strain relationship are defined as follows: σ_s^{AM}, σ_f^{AM}, ε_s^{AM} and ε_f^{AM} denote respectively the start and finishing stresses and the start and finishing strains relative to the austenite to martensite (A-M) transformation, whereas σ_s^{MA}, σ_f^{MA}, ε_s^{MA} and ε_f^{MA} are respectively the start and finishing stresses and the start and finishing strains of the martensite to austenite (M-A) transformation. The strains can be computed as a function of stresses as follows:

$$\varepsilon_s^{AM} = \frac{1}{E}\sigma_s^{AM} + \left|\varepsilon^{tr}\right| \tag{6}$$

$$\varepsilon_f^{AM} = \frac{1}{E}\sigma_f^{AM} + \varepsilon_{\max}^{tr} \tag{7}$$

$$\varepsilon_s^{MA} = \frac{1}{E}\sigma_s^{MA} + \left|\varepsilon^{tr}\right| \tag{8}$$

$$\varepsilon_f^{MA} = \frac{1}{E}\sigma_f^{MA} \tag{9}$$

The evolution of the volume fraction of martensite is determined by the equation:

$$\dot{\xi} = -(1-\xi)\frac{\dot{\varepsilon}_{eq}}{\varepsilon_{eq} - \varepsilon_f^{AM}} \tag{10}$$

for A-M transformation and by

$$\dot{\xi} = \xi\frac{\dot{\varepsilon}_{eq}}{\varepsilon_{eq} - \varepsilon_f^{AM}} \tag{11}$$

for M-A transformation where $\varepsilon_{eq} = |\varepsilon|$ is the equivalent strain.

Transformation start conditions are summarized by the following rules:

• Austenite-Martensite transformation condition

If $\varepsilon_s^{AM} < \varepsilon_{eq} < \varepsilon_f^{AM}$, $\dot{\varepsilon}_{eq} > 0$ and $0 \le \xi < 1$ then the A-M transformation takes place.

• Martensite-Austenite transformation condition

If $\varepsilon_s^{MA} > \varepsilon_{eq} > \varepsilon_f^{MA}$, $\dot{\varepsilon}_{eq} < 0$ and $0 < \xi \le 1$ then the M-A transformation is triggered.

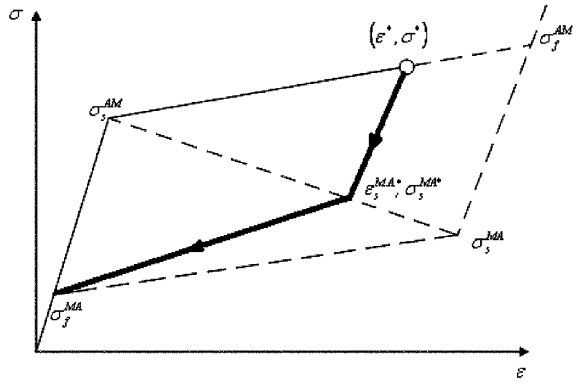

Fig. 7 Unloading path from partial loading point in copper based SMA

5.2. Case of copper shape memory alloy

In Cu-based SMA the transformation starting stress σ_s^{MA} depends on the loading history, in particular on the loading to unloading switching point (Fig. 7). Experiments reported in Trochu (1997) show that this stress can be approximated by the stress at the intersection of the top left to bottom right diagonal of the full hysteretic loop with the unloading line descending from the switching point (ε^*, σ^*) (Fig. 7).

This behavior results in the modification of the starting strain of M-A transformation from ε_s^{MA} to ε_s^{MA*} that may be calculated as a function of the switch point (ε^*, σ^*) and the switch Young modulus

$$E^* = \xi^* E_M + (1-\xi^*)E_A \tag{12}$$

5.3. Model simulation and comparison with experimental results

In the following, numerical results obtained by the proposed model are compared with experimental data presented by Casciati (2007) (Fig. 8).

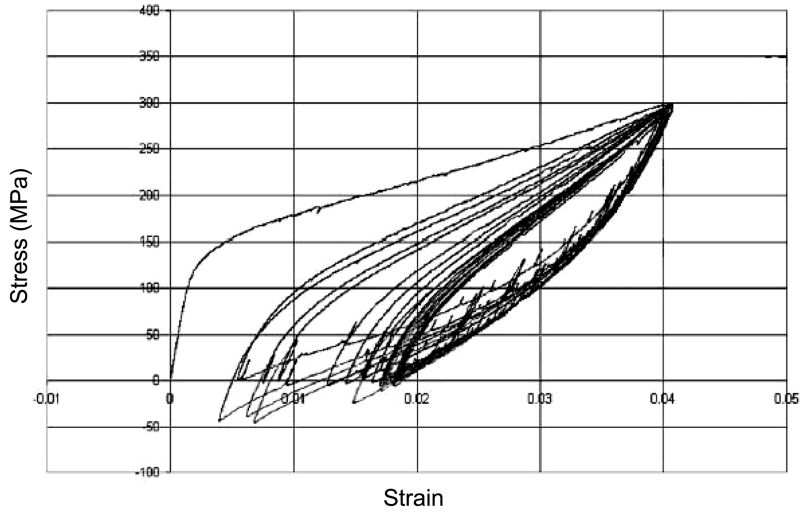

Fig. 8 Stress-strain response of a Cu-based SMA wire (after Casciati 2007)

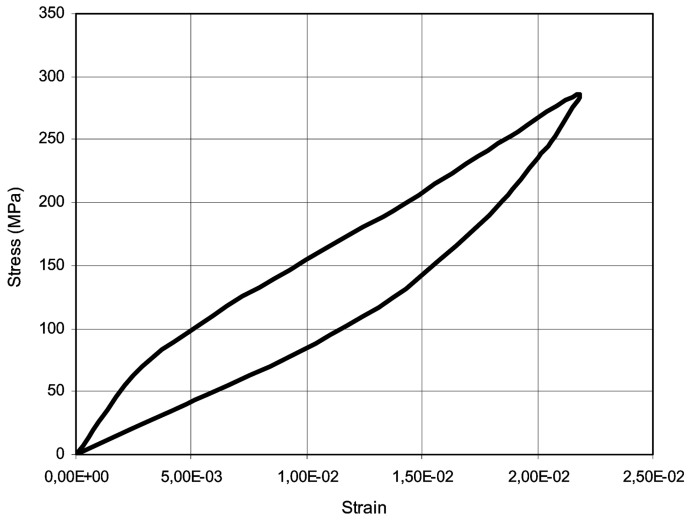

Fig. 9 Stabilized stress-strain response of a Cu-based SMA wire after 20 cycles (after Casciati 2007)

A tension test was performed on a copper based SMA wire with circular cross section of diameter 2.85 mm that was subjected to a thermal treatment. In addition, the wire was subjected, at an ambient temperature of 20 °C, to 20 loading/unloading cycles between 0% and 4% of deformation in order to reach mechanically stable cycles.

After 20 cycles, a residual strain equal to 1.85% was observed. This residual strain is taken as the new initial state and as the origin of strain for the stress-strain curve of the stabilized material depicted in Fig. 9.

From inspection of the stabilized experimental stress-strain curve the following material parameters were identified:

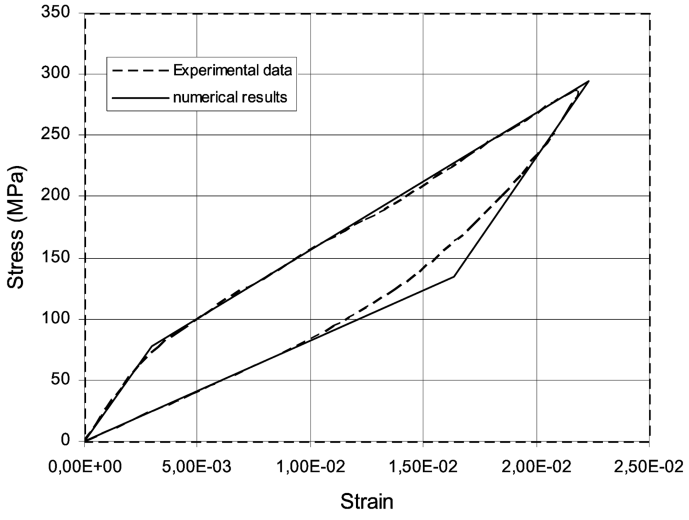

Fig. 10 Numerical results of constitutive law simulation

$E_A = 2.59\ 10^4$ MPa, $E_M = 2.59\ 10^4$ MPa, $\sigma_s^{AM} = 77.6$ MPa, $\sigma_f^{AM} = 294$ MPa, $\sigma_s^{MA} = 134$ MPa, $\sigma_f^{MA} = 0.$ MPa, $\varepsilon_s^{AM} = 3.\ 10^{-3}$, $\varepsilon_f^{AM} = 2.25\ 10^{-2}$, $\varepsilon_s^{MA} = 1.63\ 10^{-2}$, $\varepsilon_f^{MA} = 0.$

The numerical results of the tensile test are compared in Fig. 10 with the experimental data. It is clear from this figure that both sets of results are in good agreement.

6. Numerical results and discussion

6.1. Case of static monotonic loading

In order to assess the role of SMA reinforcement, a number of finite element simulations are carried out for different SMA wire sections with a given initial pretension. The applied load consists of a live load in the form of a transverse monotonic uniform pressure, combined with the dead load corresponding to the weight of the wall. In a first investigation the objective is mainly to find the adequate SMA device section which allows the wall to support a total live force of 22% of the wall weight which is equivalent to a dynamic uniform pressure having a magnitude of 0.22 g.

Fig. 11 displays the live load versus displacement curve for a node on the top surface of the wall, for different SMA wire sections without a pretension stress. The behavior is first linear then non linear up to a certain peak. The descending branch after this peak is due to the formation of cracks. The effect of SMA becomes more significant in this zone meaning that the larger is the SMA section the higher is the strength of the wall. It was concluded that the minimal section for which the wall is capable of supporting the target transverse load of 22% of the wall weight was 300 mm^2 per meter of wall length and per side. This figure also shows that the maximum transverse load that can be supported by a non reinforced wall is 14.5% of wall weight.

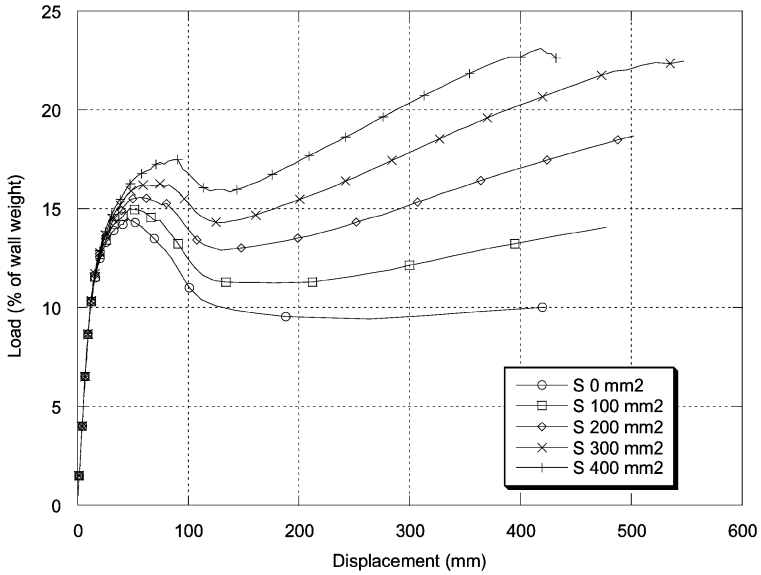

Fig. 11 Live load versus displacement for different SMA wire sections without pretension stress

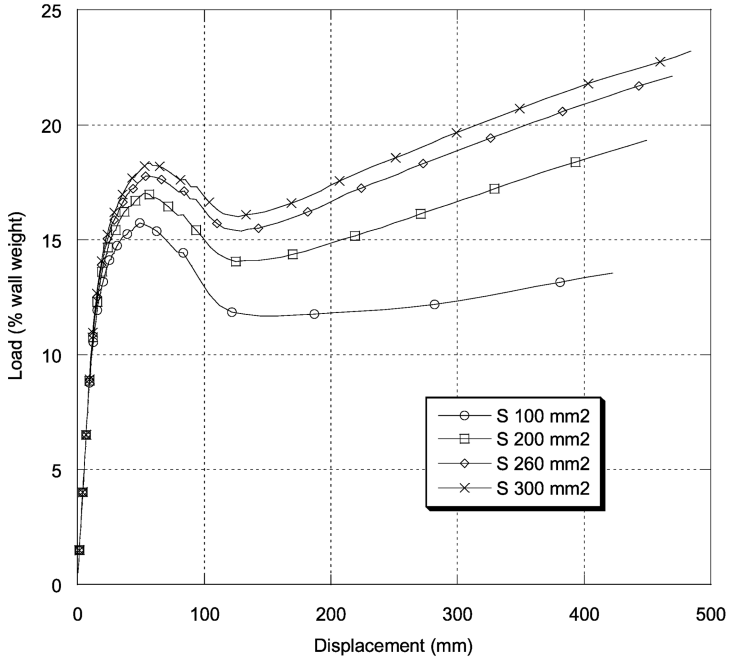

Fig. 12 Live load versus displacement for different SMA wire sections with pretension stress of 77.5 MPa

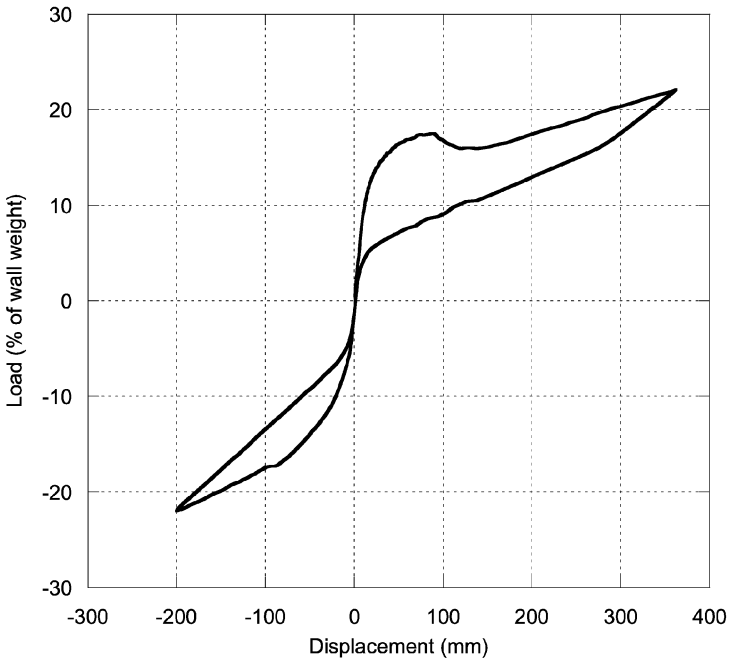

Fig. 13 Live load versus displacement in the first cycle for the wall with SMA section of 300 mm^2 per m

Fig. 12 displays the live load versus displacement curve for a node on the top surface of the wall, for different SMA wire sections with a pretension stress of 77.5 MPa. Comparing Figs. 11 and 12, it

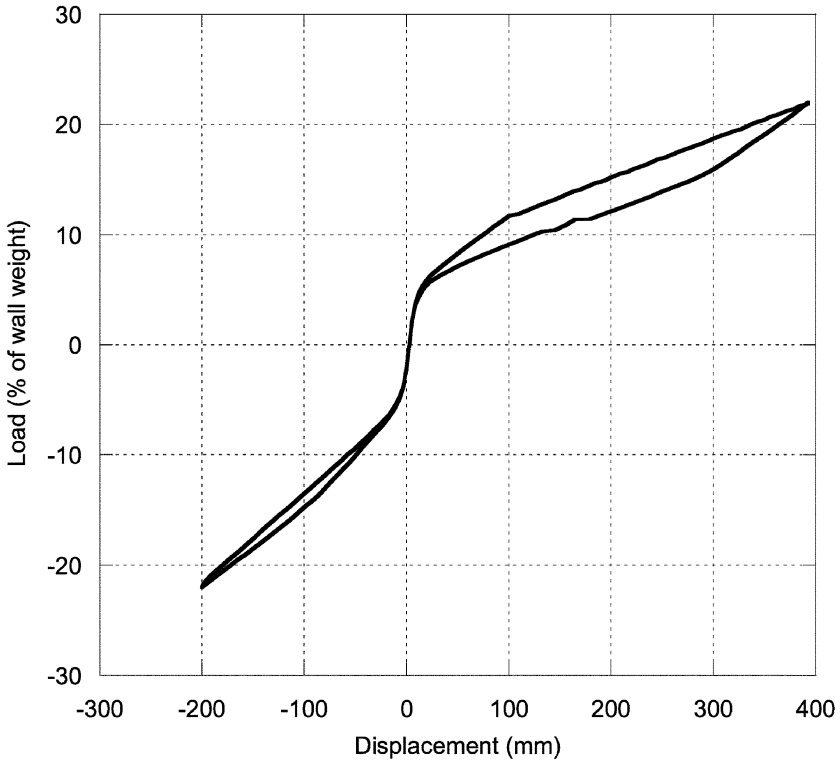

Fig. 14 Live load versus displacement in the stabilized cycle for the wall with SMA section of 300 mm^2 per m

can be seen that the initial applied pretension stress increases the maximum strengthening and the ductility of the reinforced wall. Fig. 12 shows also that the target transverse load of 22% can be supported by the wall reinforced with SMA wires of 260 mm^2 per wall length and per side section.

6.2. Case of quasi-static cyclic loading

The aim of this section is to assess the role of SMA in dissipating energy. Finite element simulations were performed for the considered wall model with SMA reinforcement section of 300 mm^2 per m of wall length and on each side. The pretension stress is set to zero and a cyclic distributed transverse load, of several cycles varying between -22% and 22% of the wall weight, are used. Fig. 13 shows the resulting load versus displacement curve for the first cycle and for a node on the top surface of the wall. It can be seen that the curve is not symmetric. The non symmetry of the curve can be explained by the occurrence of cracks during the initial loading and prior to unloading. Fig. 14 illustrates the load-displacement plot but for cycles subsequent to the third one. It is clear that the hysteretic behavior is stabilized, which indicates the damping effect of the SMA devices. This can be confirmed by the resulting stress strain curve at the base section of the SMA wires (Fig. 15).

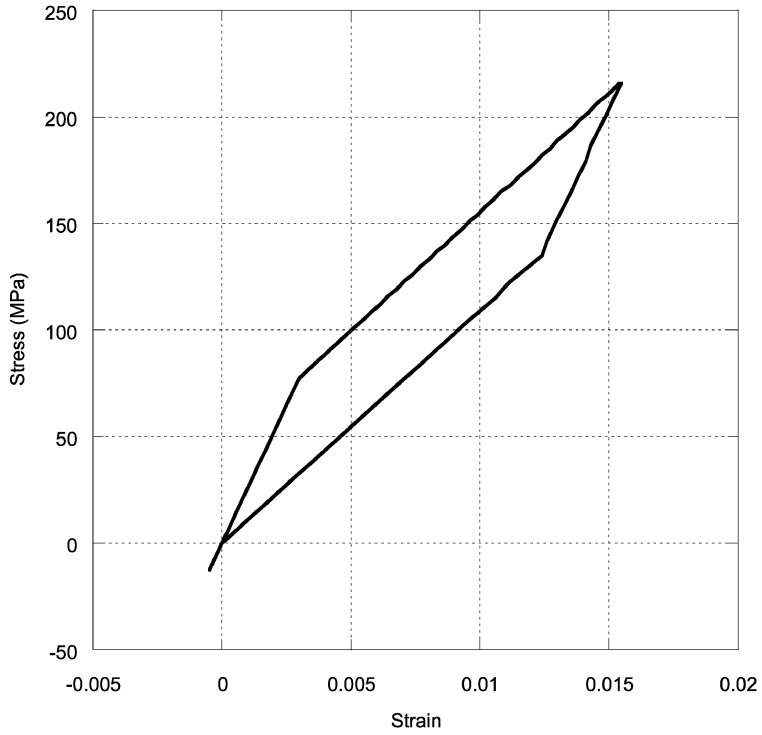

Fig. 15 Resulting strain-stress curve at base section of SMA wires in the stabilized cycles

7. Conclusions

The potential use of Cu-based shape memory alloys (SMA) in retrofitting historical monuments was studied in this paper. A finite element model of a cantilever wall in a historical monument was retrofitted with an array of copper SMA wires. A new model was proposed for heat-treated copper SMAs and was validated based on published experimental results. A series of nonlinear finite element analyses was then performed on the wall subjected to monotonic cyclic and quasi-static cyclic loadings. Simulation results show an improvement of the wall response for the case of monotonic and quasi-static cyclic loadings.

Acknowledgement

The authors are grateful for the funding provided by the European Union and Tunisia Polytechnic School. The authors are also thankful to Professor Fabio Casciati, coordinator of the FP6 European Union WIND-CHIME project.

References

Auricchio, F. and Lubliner, J. (1997), "A uniaxial model for shape-memory alloys", *Int. J. Solid. Struct.*, **34**, 3601-3618.

Boresi, A. P. and Schmidt, R. J. (2003), *Advanced Mechanics of Materials*, 6th Ed., John Wiley & Sons.
Brinson, L. C. and Huang, M. S. (1996), "Simplifications and comparisons of shape memory alloy constitutive models", *J. Intel. Mater. Syst. Struct*., **7**, 108-114.
Casciati, F. and Faravelli, L. (2007), "Structural components in shape memory alloy for localized energy dissipation", *Comput. Struct*., in press.
De Borst, R. (1987), "Smeared cracking, plasticity, creep and thermal loading: a unified approach", *Comput Meth. Appl. Mech. Eng*., **62**(1), 89-110.
El-Borgi, S., Choura, S., Neifar, M., Smaoui, H., Majdoub, M. S. and Cherif, D. (2006), "Towards a rational methodology for the seismic vulnerability assessment and retrofitting of a historical building", *Proceedings of the 4th World Conference on Structural Control*, San Diego, July.
Lagoudas, D., Rediniotis, O. and Khan, M. (1999), "Applications of shape memory alloys to bioengineering and biomedical technology", *Proceedings of the 4th International Workshop on Scattering Theory and Biomedical Applications*, Perdika, Greece, Oct., 195-207.
Patoor, E. (1990), Les alliages à mémoire de forme, Hermes, Paris.
Patoor, E. and Berveiller, M. (1994), Technologie des alliages à mémoire de forme, Hermes, Paris.
Syrmakezis, C. A., Chronopoulos, M. P., Sophocleous, A. A. and Asteris, P. G. (1995), "Structural analysis methodology for historical buildings", *Architectural Studies*, *Materials and Analysis*, Edited by C. A. Brebbia and B. Leftheris, WIT Press, 373-382.
Trochu, F. and Yao Qian, Y. (1997), "Nonlinear finite element simulation of superelastic shape memory alloy parts", *Comput. Struct*., **67**, 799-810.

FC